Proceedings World Geothermal Congress 2020+1
Reykjavik, Iceland, April - October 2021

Advances in Structural Understanding in Northern Sarulla, North Sumatra, Indonesia from Analysis of LiDAR Images

Phil White, Julie Rowland and Yudha Satya

pwhite@pandageoscience.co.nz

Keywords: Sarulla, LiDAR, structure, permeability, sector collapse

ABSTRACT

Geothermal exploration and structural mapping at Sarulla in the 1990s was difficult due to the thick forest cover, steep terrain, and limited resolution of remote sensing techniques. When LiDAR images were obtained in 2015, many new faults were identified and mapped, and a major sector collapse became visible at Namora-I-Langit. Here we present the results of this work, which has been updated through recent review and further structural analysis. The Sumatra Fault Zone (SFZ) is seen to comprise a network of major faults that strike between N-S and NNW-SSE, along with complex horsetails and sinuous linking faults between the major structures. The SFZ is cut by cross faults that are almost perpendicular to it, and an older set of ENE-WSW faults is also visible. The sector collapse at Namora-I-Langit has exposed the clay cap over an area that is up to 2 km wide by 5 km long, and this area hosts over 90% of the thermal features.

In forested terrain like Sarulla, LiDAR images are a very quick, cost effective and accurate way of analysing geomorphology and structural features. In such areas, having LiDAR images available at an early stage should be considered as essential as MT geophysical surveys prior to siting wellpads and targeting wells.

1. INTRODUCTION

LiDAR (Light Detection and Ranging) is a remote sensing method that uses light to measure ground elevations and produce an accurate three-dimensional digital elevation model (DEM), which is generally presented as a shaded topographic image. The technology has been available for more than 50 years, though it is only in the last 10 years that it has become more commonplace in the geothermal industry. LiDAR surveys can be flown by fixed wing aircraft or helicopters, and now by drones, giving cost-effective topographic surveys.

For geothermal exploration, the advantage of LiDAR over other remote sensing methods is that LiDAR can detect the ground surface through vegetation, including dense forest, and gives high resolution data, so it is now possible to obtain an accurate DEM that reveals structures which were previously hidden. Understanding the orientation and location of structures is one of the key aims of geothermal exploration prior to drilling. A good structural understanding provides greater confidence in siting the power plant and wellpads, and more success in targeting wells to intersect permeable structures in both production and injection areas.

Here, a case study is presented which highlights the usefulness of LiDAR for identifying structures at the Sarulla geothermal project.

2. SARULLA GEOTHERMAL PROJECT

2.1 Location and History

The Sarulla contract area is located in North Sumatra, and extends from approximately 40 to 100 km south of Lake Toba (Figure 1). The area includes four separate geothermal systems, from north to south: Namora-I-Langit (NIL), Silangkitang (SIL), Donotasik and Sibualbuali. This discussion covers only Namora-I-Langit and Silangkitang. Namora-I-Langit is 3-4 kilometres west of the SFZ and just 10 km NW of Silangkitang, which is situated directly on the SFZ.

Sarulla was explored by Unocal North Sumatra Geothermal (Unocal) from 1993 to 1997, but after the 1998 Asian financial crisis, the concession was acquired by the state-owned electricity company PLN. In 2006, the Sarulla Operations Limited (SOL) consortium of Ormat Technologies Inc. (Ormat), P.T. Medco Power Indonesia (Medco) and Itochu Corporation (Itochu) won the rights to develop the field, with Kyushu Electric Power Co. Inc. (Kyushu) and Inpex Corporation (Inpex) later joining the group. After the Power Purchase Agreement was amended in 2013, drilling and construction commenced in 2015. The first 110 MWe unit at Silangkitang (SIL) began commercial operations in March 2017, and the two 110 MWe units at Namora-I-Langit (NIL) began production in October 2017 and May 2018.

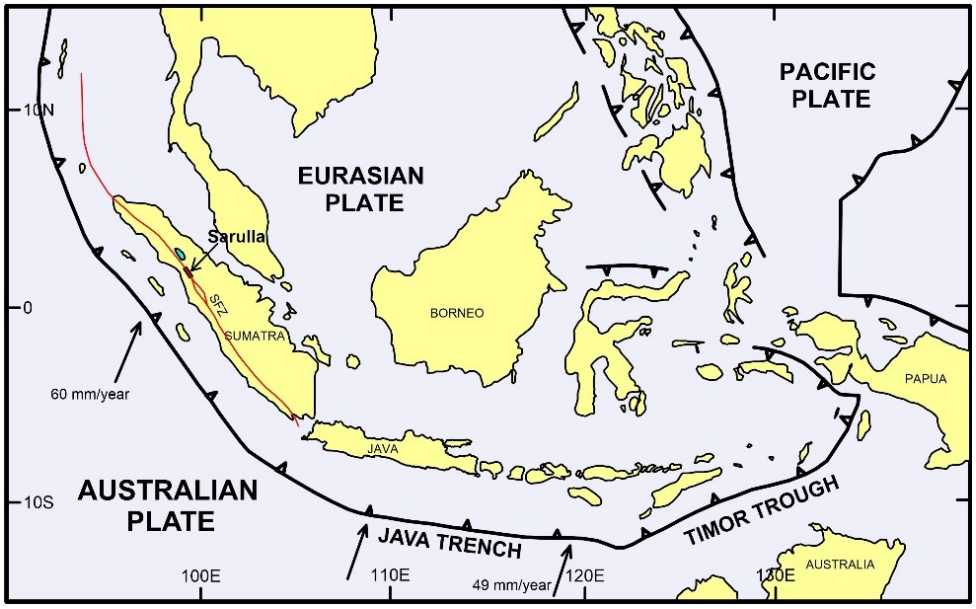

Figure 1: Tectonic map of Indonesia (Hamilton 1981), showing the location of Sarulla on the Sumatra Fault Zone (SFZ).

2.1 Geological Setting

Sarulla is situated within the Sunda volcanic arc, where Miocene to present volcanic activity is associated with oblique subduction of the Indo-Australian plate beneath Sumatra at the Sunda trench (Figure 1). The oblique component of subduction is largely accommodated on the dextral Sumatra Fault Zone (SFZ), which is spatially associated with the volcanic arc. Slip rates of around 25 mm/year occur in the vicinity of Sarulla (Hickman *et al.* 2004).

Surface geology is dominated by the products of Quaternary arc volcanism overlying older volcanic and sedimentary rocks (Aspden *et al*. 1982, Gunderson *et al*. 1995, 2000). The young volcanic material includes widespread rhyolitic ash of the 73 ka. Young Toba Tuff, originating from an eruption of Lake Toba caldera to the north, along with predominantly dacite-rhyolite volcanic complexes. Beneath the young volcanic material are folded and faulted Paleozoic metasediments and Tertiary sedimentary rocks on the eastern side of the SFZ, and Tertiary volcanics and Mesozoic to Tertiary intrusive rocks on both sides of the SFZ. All of these units are affected by dextral strike-slip faulting within the NW-SE trending SFZ, which has been active since at least the mid Miocene (Hall 1996). The basement rocks are also cut by older structures.

Steep terrain, thick forest cover, a widespread blanket of young pyroclastic deposits, and sparse outcrops make field mapping at Sarulla very challenging. There are few if any exposures with direct evidence of faulting (*e.g.* fault breccias, striated fracture surfaces), and the best field evidence for the presence of faults is in Silangkitang, where some of the thermal features are aligned.

2.3 Previous Structural Models

During exploration in the 1990s, Unocal undertook extensive field mapping, sampling and analysis of fresh and altered rocks and thermal features, plus resistivity and gravity surveys (*e.g.* Gunderson *et al*. 1995, 2000, Moore *et al*. 2001, Hickman *et al*. 2004). Structural features were examined in the field and using satellite imagery, and in addition to the "principal strand" of the Sumatra Fault System, Gunderson *et al* (1995) noted "… numerous small subsidiary parallel and antithetic (tensional/extensional) faults, as evidenced by common minor fault scarps and sag ponds", though few of these were mapped. With the data and methods available at the time, the Unocal team identified just four NNW striking faults and one almost perpendicular structure at NIL (*e.g*. Ganefianto 1998). The structural interpretation of Unocal (Figure 2) was used with minor modification by SOL for all well siting and well targeting until LiDAR images became available in 2015.

2.4 Downhole information

Namora-I-Langit

Good permeability was found in all of the NIL production and injection wells, despite limited evidence of faulting at the surface in this area. The average initial output of the NIL production wells was 30 MWe (900 tonnes per hour (tph) steam + brine) and the injection wells had an average capacity of 1100 tph.

In 2016, a downhole acoustic (ABI) image log was obtained from well WJP1-3, in the south of NIL, over the interval 1828-2133 m. Additional logging would have been undertaken but was stymied by unstable formations in the reservoir section of many wells. The log from WJP1-3 indicates that the majority of structures in this well strike NNE and dip to the east at 50-70° from vertical (Figure 3). This means that they are at an angle to the NW trending SFZ, and to the NW faults that were postulated by Unocal. In the big picture these structures identified in WJP1-3 are subparallel to the relative plate motion vectors (Figure 1), and therefore should be extensional. However, there is a wide range of orientations, including in the main feedzones, some of which are close to N-S, while others are almost E-W. As will be seen below (Figure 4), the structural orientations in WJP1-3 are consistent with what was interpreted from the LiDAR image.

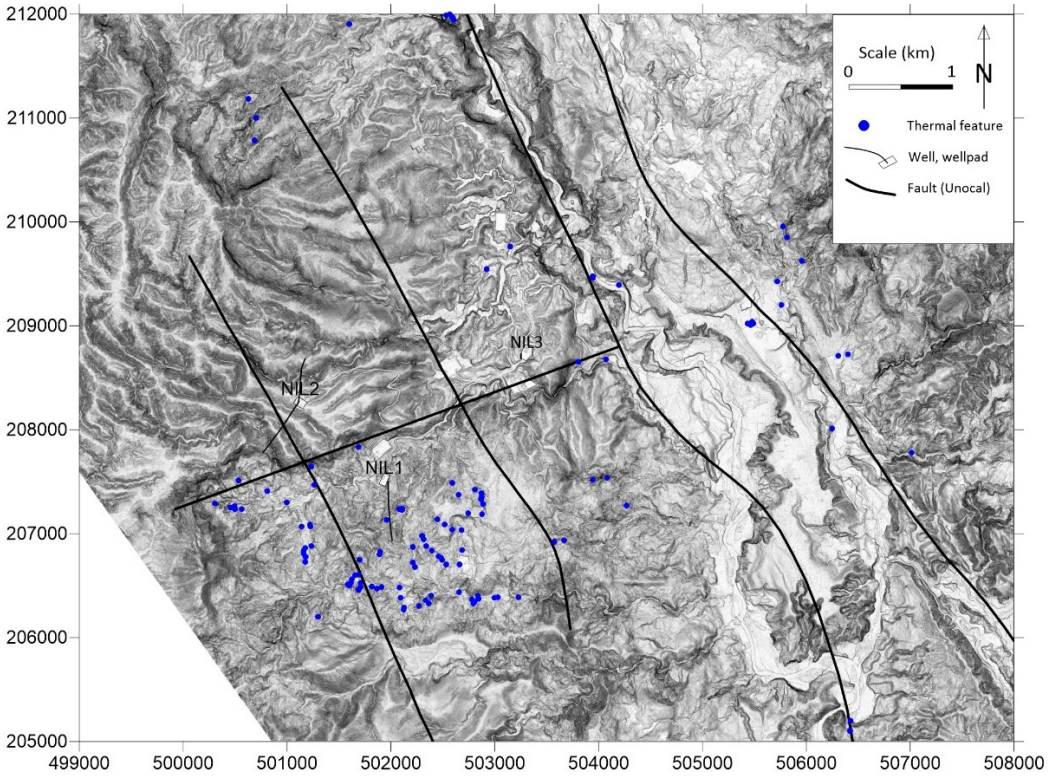

Figure 2: Faults identified by Unocal (Ganefianto 1998) in Namora-I-Langit, superimposed on the LiDAR image. Also shown are thermal features and the wells drilled by Unocal (NIL1, NIL2-1, NIL2-2 and NIL3 (vertical)).

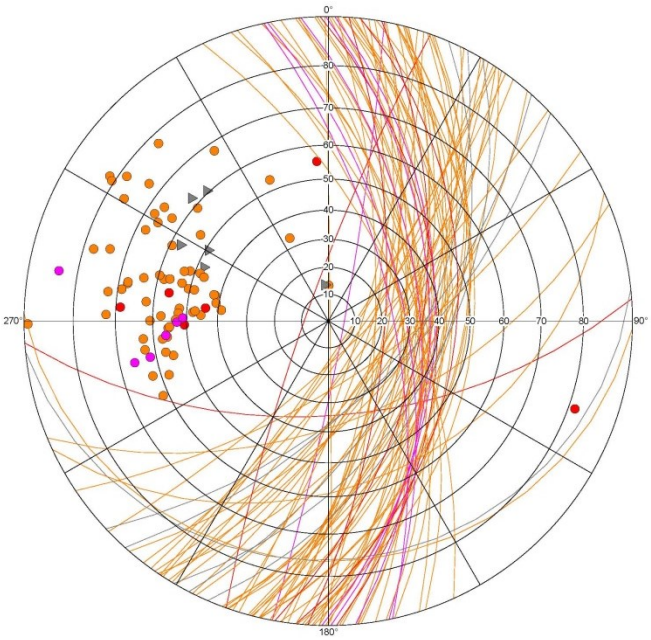

Figure 3: Stereonet plot of structures identified in the acoustic image log of WJP1-3 (image Peter Drakos, pers. comm. 2016). Red circles = major open joint/fracture, pink circles = minor open joint/fracture, orange circles = partially open joint/fracture, grey triangles = undifferentiated/broken zone.

Silangkitang

At SIL, the four production wells are all drilled eastward into the Sumatra Fault Zone, and all four are highly productive. The average initial measured output was 53 MWe (over 1000 tph steam + brine) based on individual well tests. Injection wells were drilled from three wellpads: two of those (SIL2 and SIL3) drilled east and also found good permeability on the SFZ. The best permeability is in the wells on SIL2 pad, which drilled into several N-S oriented horsetail fault strands (Figure 5). Despite fears that there would be rapid injection returns to the production area along the SFZ, tracer testing after less than a month of operation showed very limited tracer returns. Two injection wells (plus a sidetrack) that were drilled to the west (away from the SFZ, in an area without identified fault targets) from the SIL1N pad (Figure 5), had very low injectivities.

3. INTERPRETATION OF LIDAR IMAGERY

An airborne LiDAR survey was undertaken over 165 km^2 in the northern part of the contract area in 2015, covering the NIL and SIL projects that were being drilled and developed at the time. The LiDAR DEM from this 2015 survey was used for the present study. It has a horizontal resolution of <0.3 m, and a vertical resolution of <0.15 m. In 2017, a survey of an additional 441 km^2 extended LiDAR coverage to the southern limit of the contract area.

3.1 Geological Units

Where geological units are young and well preserved, various lithologies, including individual lava flows, can be identified from LiDAR images (*e.g.*, Kereszturi *et al*., 2018). However at Sarulla, there are few distinctive lithological features visible on the LiDAR image, other than alluvial terraces and in places, smooth rounded ridges on siliceous domes of rhyolite/dacite. This may be partly due to weathering and erosion, and also to the effect of the young ash deposits (especially the Young Toba Tuff) that have smoothed the topography and infilled any craters that may have been present.

3.2 Sector Collapse

An area of irregular topography that contrasts with the smooth rounded topography elsewhere is apparent in the south of Namora-I-Langit on the LiDAR DEM (Figure 4). This area measures some 5 km long by up to 2 km wide, and ranges in elevation from about 1000 masl in the west to about 600 masl in the east. It is elongate parallel to the slope, and approximately 100 m lower in elevation than the land to either side. Based on all of these features that were evident from the LiDAR image, this was interpreted as a sector collapse. In addition, the vast majority of thermal features at NIL are located within this area. Other evidence indicates that failure occurred at about the level of the electrically conductive and mechanically weak smectite clay-rich layer above the geothermal reservoir. That evidence comprises:

- The MT profiles indicate that the top part of the geothermal system is missing here, with the conductive layer almost at the surface, whereas in surrounding areas, the conductor is beneath a layer of moderate resistivity.
- Outside this area, the highest methylene blue (MeB) values, which correspond to the highest smectite clay contents, occur 200-500 m below the surface, whereas wells drilled from within the sector collapse (on WJP1 and NIL1N pads) have peak MeB values within 100 m of the surface.

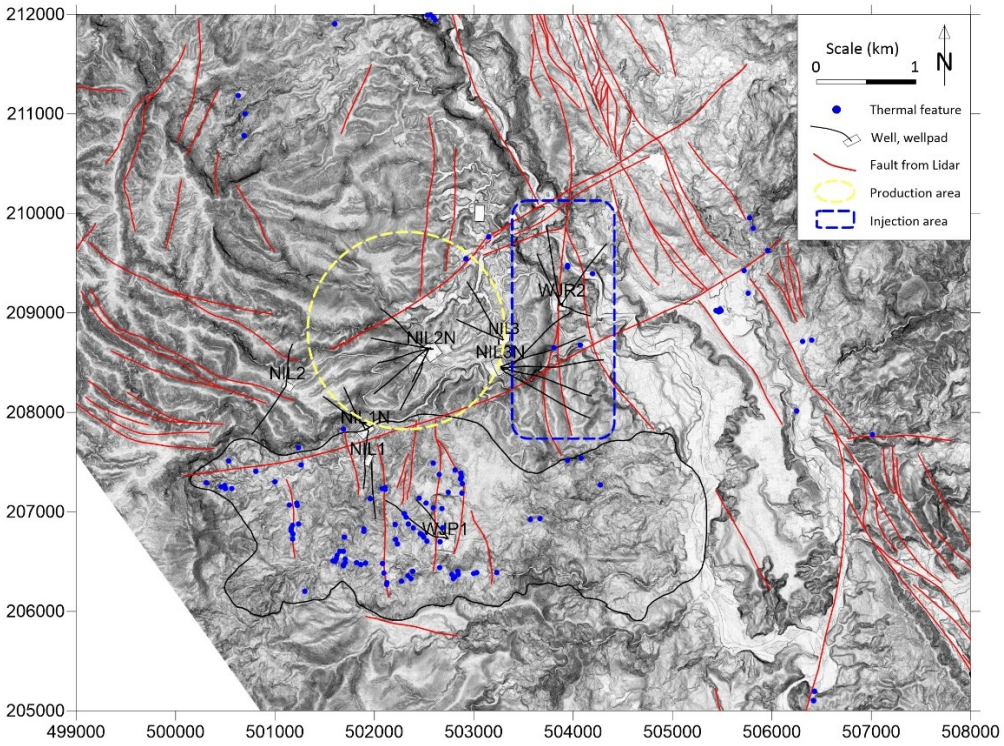

Figure 4: LiDAR image of Namora-I-Langit area, showing production and injection areas, all wells, thermal features, sector collapse (outlined in black), and faults inferred from the LiDAR image.

3.3 Faulting

Namora-I-Langit

From analysis of the LiDAR image, many possible fault structures with a range of orientations have been identified (Figure 4). In the east of the area, a set of closely spaced NW to NNW oriented structures are visible, and together these constitute the Sumatra Fault Zone. In contrast to a few large continuous structures identified previously (Figure 2), the SFZ is now seen to comprise many small interlinked structures, each of which extends for a few hundred metres to a few kilometres. Associated with these NW to NNW trending structures, there are a number of splays and linking faults with an approximately N-S orientation, as identified by Gunderson *et al* (1995). These N-S structures become more common away from the main SFZ.

In addition, two significant NE-SW structures are visible at NIL. These NE-SW structures terminate or offset some of the NW to NNW faults, although others are continuous across them. One of the NE structures coincides with the northern margin of the sector collapse, and may have played a part in the formation of that collapse (Figure 4).

To the west of NIL, where less influence from the Sumatra Fault Zone would be expected, a few WNW oriented structures are visible on the LiDAR image. These may represent an older set of structures, possibly related to pre-Miocene continental accretion (*e.g.* Metcalfe 2017).

There is a notable lack of visible structures above the main NIL production area on LiDAR, despite all of the production wells finding good permeability at depth. It could be inferred from the predominantly NNE structures in surrounding areas, particularly to the north and east, that this is also the main orientation of structures beneath the production area, as was confirmed by the acoustic image logging.

Silangkitang

At SIL, faults inferred from the LiDAR image are broadly consistent with the Unocal fault maps (Figure 5), although there are differences in the detail. In the LiDAR interpretation, several of the NW strands terminate at N-S trending horsetails (*e.g.* near SIL2N), and there are lateral sidesteps between strands. At SIL, NW-SE faults (parallel to the SFZ) and N-S splays and cross-faults are both common, in contrast to NIL, where N-S and NE-SW faults are important in the reservoir. The SIL geothermal system is strongly structurally controlled, with the hottest part of the system occurring on the SFZ near the SIL1 wells.

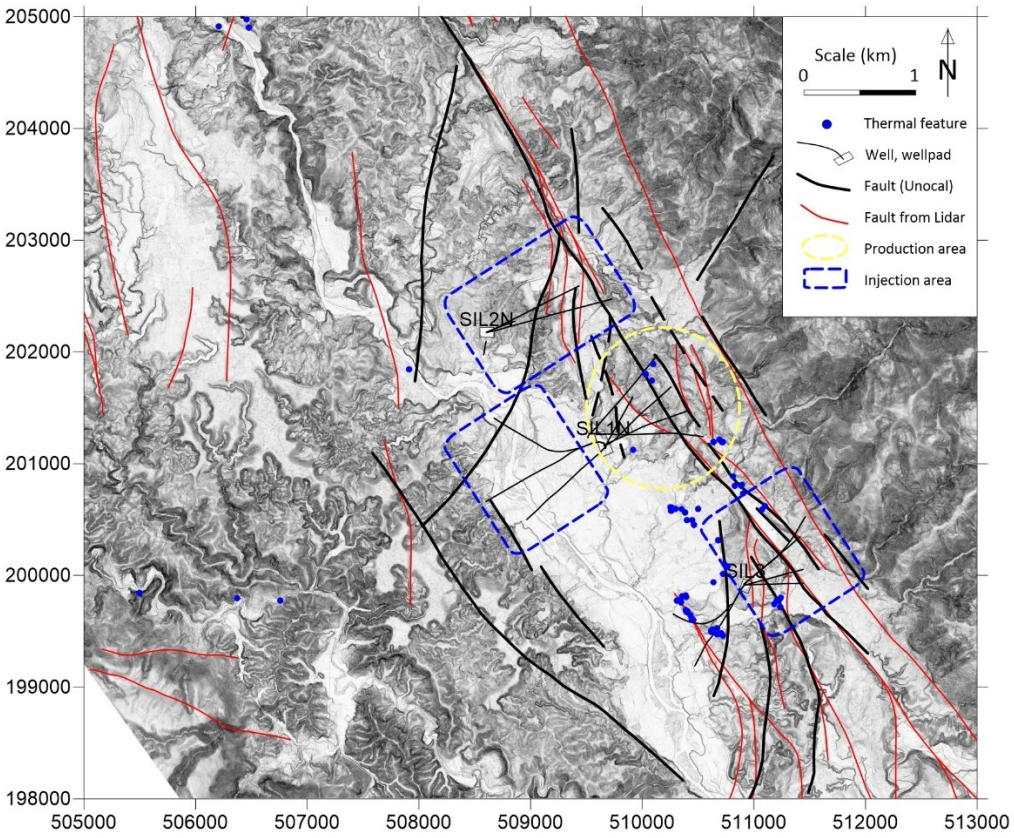

Figure 5: LiDAR image of Silangkitang area, showing production (yellow circle) and injection areas (blue rectangles), well tracks, thermal features, and possible faults from Unocal (Melosh and Molling 1995) and from the LiDAR image.

4. DISCUSSION

Having a LiDAR DEM has led to a much improved structural understanding of the NIL and SIL geothermal systems at Sarulla. The reasons for the better permeability of some wells and the lower temperature of others can now be explained in terms of the structural model. With the benefit of hindsight, some decisions would have been different, and the development might have been more efficient if the LiDAR images been available at an earlier stage of the geothermal project.

4.1 Wellpads

Almost all of the wellpads at Sarulla were sited before the LiDAR images were available. Some of those wellpads would have been located differently if the LiDAR images had been available earlier. Two specific examples are:

4.1.1 WJR2

LiDAR images indicate the presence of a fault crossing the western side of the WJR2 injection pad at NIL. This fault appears to dip to the east beneath the pad. Most of the wells drilled on this pad encountered shallow losses between 150 and 800 m depth,

which caused drilling difficulties and delays in each of those wells. Simply moving the cellars 50 m to the west to locate them on the footwall side of the fault may have avoided these problems.

4.1.2 WJP1

The sector collapse at NIL was never recognised prior to the availability of LiDAR images of the area. Where sector collapses have been observed in other geothermal systems, not only is it easier for steam to reach the surface, but it is also easier for cool fluids to descend into the reservoir (*e.g.* Lihir, PNG - White *et al*. 2010), meaning that the part of the geothermal system beneath a sector collapse will be less viable for power generation. There is evidence that the reservoir at NIL has cooled beneath the sector collapse, where low temperatures were found in the first (vertical) well drilled on the WJP1 wellpad.

Had the sector collapse been recognised earlier, the WJP-1 wellpad might not have been constructed, and the wells that were drilled from this pad would have been drilled elsewhere.

4.2 Well targeting

The production wells at NIL were mostly drilled before the LiDAR data was available, and those wells were targeted based on the NW fault orientation from the Unocal structural model. From the LiDAR image, there are few clear structural targets within the NIL reservoir, but NNE faults are common to the north and it is assumed that faults of similar orientation will be present within the reservoir.

The NIL production wells were drilled between southwest and northwest, and all of these wells were productive, but the well with the highest productivity (NIL2N-2) was drilled to the NW, so is essentially parallel to the Unocal faults (Figure 2), but almost perpendicular to the NNE extensional faults from LiDAR (Figure 4). NIL2N-2 may have also reached one of the NE-SW faults on the LiDAR map, which further contributed to its high productivity. Likewise, the least productive wells were NIL2N-7 (drilled to the SSW, *i.e.* parallel to the NNE LiDAR faults) and NIL2N-6 (vertical). Hence, the observed well productivities are more consistent with the LiDAR interpretation than the previous fault map. Two new wells that were drilled to the NW from the NIL3 wellpad were both productive, and this remains the favoured orientation for future wells at NIL.

The NIL injection wells were drilled to the north and east, where the LiDAR image indicates there are both N-S and NE-SW faults. Most of these injection wells encountered good permeability, with the best permeability found in wells that were targeted using the LiDAR data, and which likely intercepted both sets of faults (*e.g*. WJR2-4, NIL3N-2 and NIL3N-3).

Most of the SIL wells were drilled prior to the LiDAR surveys, and most were drilled to the east into the main SFZ, and were very permeable, and highly productive. Only the injection wells that were drilled to the west encountered low permeabilities. This includes SIL1N-5, 5ST and 6, which were drilled into an area where no structures are visible on the LiDAR DEM, although the Unocal structural map suggested that SIL1N-5 and SIL1N-5ST might have reached faults. However two new wells that were drilled to the SW from the SIL3 wellpad with the benefit of the LiDAR data toward identified faults and beneath thermal features had low permeability, meaning that success is never guaranteed.

4.3 Other Benefits of LiDAR

In addition to identifying and avoiding faults and sector collapse structures, using an accurate 3D LiDAR model, it is possible to undertake preliminary civil design works by determining the gradient of possible access routes and calculating cut volumes for potential wellpads and power plant sites even before visiting those sites in the field.

CONCLUSIONS

LiDAR images are a very cost effective and accurate way of revealing geomorphological and structural features, especially in areas of dense vegetation and steep topography with difficult access. They may reveal features that are difficult or impossible to identify in the field, with air photos or from satellite imagery.

At Sarulla, many new fault traces and a major sector collapse were first identified from LiDAR images. The new structural interpretation of mostly N to NNE oriented extensional faults within the NIL reservoir is quite different from the previous model of largely NW oriented faults. The Sumatra Fault Zone (SFZ) is seen to comprise a network of major faults that strike between N-S and NNW-SSE, along with complex horsetails and sinuous linking faults between the major structures. The SFZ is cut by cross faults that are almost perpendicular to it, and an older set of ENE-WSW faults is also visible. The sector collapse at Namora-I-Langit has exposed the clay cap over an area that is up to 2 km wide by 5 km long.

If the LiDAR images had been available at an earlier stage of development at Sarulla, some wellpads would have been sited better, and wells would have been targeted to intersect permeable structures with greater confidence. We recommend that for most geothermal projects, obtaining and analysing LiDAR images should become a routine part of geothermal exploration prior to drilling, in the same way that MT resistivity surveys are.

ACKNOWLEDGEMENTS

The authors are grateful for the support and permission from Sarulla Operations Limited to publish the material in this paper. We also wish to acknowledge the many individuals and groups who have contributed to the successful drilling, construction and commissioning of units 1 to 3 at Sarulla.

REFERENCES

Aspden, J.A., Kartawa, W., Aldiss, D.T., Djunuddin, A., Diatma, D., Clarke, M.C.G., Whandoyo, R., and Harahap, H.: Geological map of the Padangsidempuan and Sibolga Quadrangles, Sumatra. Pusat Penelitian dan Pengembangan Geologi, Bandung (1982).

Ganefianto, N.: NIL 1-1 geologic summary. Unpublished Unocal report (1998).

Gunderson, R.P., Dobson, P.F., Sharp, W.D., Pudjianto, R., and Hasibuan, A.: Geology and thermal features of the Sarulla Contract Area, North Sumatra, Indonesia. *Proceedings* World Geothermal Congress (1995), 687-692.

Gunderson, R., Ganefianto, N., Riedel, K., Sirad-Azwar, L., and Suleiman, S.: Exploration results in the Sarulla block, North Sumatra, Indonesia. *Proceedings* World Geothermal Congress (2000), 1183–1188.

Hall, R.: Reconstructing Cenozoic SE Asia. In: Hall, R & Blundell, D.J. (eds.) *Tectonic evolution of SE Asia*. Geological Society of London Special Publication 106: 153-184 (1996).

Hamilton, W.: Tectonic map of the Indonesian region 1:5,000,000. USGS Miscellaneous investigations series Map I-875-D (1981).

Hickman, R.G., Dobson, P.F., van Gerven, M., Sagala, B.D., and Gunderson, R.P.: Tectonic and stratigraphic evolution of the Sarulla graben geothermal area, North Sumatra, Indonesia. *Journal of Asian Earth Sciences* **23** (2004), 435-448.

Kereszturi, G., Shaefer, L.N., Schleiffarth, WK., Proctor, J., Pullanagari, RR., Mead, S., and Kennedy, B., 2018. Integrating airborne hyperspectral imagery and LiDAR for volcano mapping and monitoring through image classification. *International Journal of Applied Earth Observation and Geoinformation* **73**: 323-339.

Melosh, G., and Molling, P.: Silangkitang 1-2 completion report. Unpublished Unocal report (1995).

Metcalfe, I.: Tectonic evolution of Sundaland. *Bulletin of the Geological Society of Malaysia* **63**: 27-60 (2017).

Moore, D.E., Hickman, R.G., Lockner, D.A., and Dobson, P.F.: Hydrothermal minerals and microstructures in the Silangkitang geothermal field along the Great Sumatran fault zone, Sumatra, Indonesia. *Geological Society of America Bulletin* **113** (2001), 1179-1192.

White, P., Ussher, G., and Hermoso, D.: Evolution of the Ladolam Geothermal System on Lihir Island, Papua New Guinea. *Proceedings* World Geothermal Congress, Bali (2010).

Wolf, N., Gabbay, A.: Sarulla 330 MW geothermal project: key success factors in development. *Proceedings* World Geothermal Congress, Melbourne, Australia (2015).